Proceedings of the 16th European Turbomachinery Conference (ETC16)
Turbomachinery, Fluid Dynamics and Thermodynamics,
March 24-28, 2025; Hannover, Germany

CFD analysis of an optimized tilted H-shaped VAWT at three different scales

O. Kouaissah *[1], N. Franchina[1], M.S. Siddiqui[2], H.H. Mian[2], and G. Persico[3]

[1]Dipartimento di Ingegneria e scienze applicate, Università degli Studi di Bergamo, Viale Marconi 5 - 24044 Dalmine (BG), Italy
[2]Faculty of Science and Technology, Norwegian University of Life Sciences, 1430, As, Norway
[3]Dipartimento di Energia, Politecnico di Milano, via Lambruschini 4 - 20156, Milano

Abstract

Wind energy will play a key role in cost-effectively meeting decarbonization objectives as suggested by the continuous growth of research projects on wind turbines presented in the last decades. Several recent numerical and experimental studies have highlighted that lift-driven vertical axis wind turbines (VAWTs) are well-suited for the emerging floating off-shore wind market. VAWTs have the potential to reduce both installation and maintenance costs, while also offering improved wake recovery. Despite VAWTs advantages, the flow field developing around the rotor is inherently unsteady, fully three-dimensional, and characterized by complex interaction between blades and vortical structures arising during rotor revolution. High resolution computations are cornerstone in the design, assessment, evaluation phases. In this work, we present a 3D study on the performance of an optimized straight-blade H-shaped VAWT. The wind rotor has been designed using results coming from a former study. The blades features are conceived to better deal with flow characteristics typical of a tilted condition, common in floating offshore applications. The VAWT performance has been computed at peak power condition, at three different scales, ranging from a small laboratory model towards a large-scale one. The effective power harvesting capability is a key issue to promote actual installations; the results aim at estimating the viscous losses due to Reynolds effect. Local and global flow features are deeply discussed to shed light on the wind rotor capability. Furthermore, the near-wake development is considered in tight connection to the vortices developing within and behind the rotor as a function of selected design parameter, namely the blade coning angle and the static tilt angle applied. **Keywords**: Optimized-VAWT, tilted-VAWT, Scaled-VAWT, Near-Wake, URANS-CFD.

1 Introduction

Offshore wind energy is increasingly recognized as a key solution for renewable power generation. Offshore wind turbines, located far from shore, take advantage of stronger, more consistent wind conditions while minimizing human impact, reducing land use, and decreasing both noise and visual pollution. In 2023, 25 new offshore wind farms were brought online, adding 9.8 gigawatts (GW) to global capacity, bringing the total to 67.4 GW [1]. The majority of this capacity is supported by fixed-bottom structures in waters shallower than 60 meters [2]. However, around 80% of the world's offshore wind potential exists in waters deeper than 60 meters [3], where only floating platforms are viable, highlighting the need for cost-effective technologies that can operate in these deeper environments. Currently, all floating offshore wind turbine (FOWT) prototypes use horizontal axis wind turbines (HAWTs). The Levelized Cost of Energy (LCOE) for floating wind varies widely, depending on factors such as the floater typology, wind conditions, seabed depth and characteristics, and distance from shore. Reducing the LCOE of current floating HAWTs requires overcoming challenges like scaling limitations, wake effects, and operations and maintenance (O&M) costs [2]. Vertical Axis Wind Turbine (VAWT) technology offers several advantages that make it particularly attractive in floating offshore applications. One key benefit is the placement of heavy components at lower levels, which enhances structural stability and reduces costs related to installation, operation, and maintenance. Unlike HAWTs, VAWTs do not require a yaw control system, as their design inherently allows for omnidirectional operation [4]. Additionally, VAWTs present the opportunity to use a direct-drive generator (DDG) instead of a complex speed-increasing multistage gearbox, which is often a source of failure in HAWTs [5]. Field studies have shown that the wakes of an array of counter-rotating VAWTs can be mitigated, and mixing can occur over a reduced distance, potentially improving overall power harvesting [6]. Moreover, VAWTs can be scaled up for floating offshore applications with fewer significant obstacles compared to HAWTs. Enabling the construction of substantially larger rotors than the actual HAWTs. Estimates suggest that VAWTs' maximum potential, considering structural integrity aspects, can reach around 30 MW [7]. As a result, it was estimated that a well-designed floating VAWT with an optimized platform and efficient mooring system could reduce the LCOE by more than 20% compared to the traditional floating HAWTs [8]. It is widely recognized that one of the primary goals of VAWTs is to improve performance in offshore applications. To achieve cost-effective and viable VAWT farms, large multi-megawatt (MW) turbines are essential. However, scaling up to large turbines presents several significant challenges: i) the performance of small-scale models must be carefully evaluated against real-world flow conditions, as Reynolds number effects can influence the actual energy harvesting capability; ii) aeroelastic instabilities may also affect the turbine's structural integrity. Addressing these challenges from both aerodynamic and structural perspectives is crucial for developing innovative Darrieus VAWT designs and ad-

*Corresponding author: otman.kouaissah@unibg.it, tel. +39-035-2052084

vancing the deployment of multi-megawatt wind farms. Several studies in the literature have highlighted technical solutions that can facilitate the installation of large-scale VAWTs, as reported in works such as [9–11].

VAWTs are generally configured in an upright orientation. However, when installed on spar-buoy platforms, having a low center of gravity, they can operate in a tilted position. While the upright configuration has been the focus of extensive research, the aerodynamic and operational characteristics of VAWTs in a tilted state have been addressed in only a limited number of studies. Mertens et al. [12] analyzed the effects of mounting a two-bladed H-shaped VAWT on urban rooftops, emphasizing the impact of skewed airflow caused by the non-horizontal wind direction at roof level. Wind flow at the top of tall buildings often inclines at an angle of 10 to 20 degrees relative to the horizontal plane. This study observed a performance increase of about 30% for VAWTs with skew angles ranging from 20 to 30 degrees [12]. Ferreira et al. [13, 14] investigated the behavior of two-bladed H-Darrieus rotors in both skewed and non-skewed flow conditions. They measured aerodynamic thrust and flow velocity, confirming that skewed flow conditions alter the aerodynamic forces, contributing to increased power generation. This extra power is primarily concentrated in the downwind section of the VAWT's rotation, particularly in the area not affected by the wake generated during the blade's upwind passage. Extensive experiments were conducted on Troposkien-shaped VAWTs using the small-scale DeepWind demonstrator, considering various wind speeds, rotor angular velocities, and a 15-degree tilt arrangement [15]. Unlike the H-shaped turbine, the Troposkien VAWT showed reduced performance in skewed flow conditions compared to the upright configuration. In addition to these few experimental results, computational studies have been conducted on skewed or tilted VAWTs over the past decade. Wang et al. [16] suggested modifications to the double multiple streamtube model to simulate the performance of a tilted rotor. Scheurich and Brown [17] utilized a vorticity transport model to simulate the aerodynamic performance and wake dynamics of various VAWT designs under both skewed and non-skewed flow scenarios. They observed that in skewed flow conditions, the wake exhibits oblique convection, allowing portions of each blade to operate undisturbed in the downwind regions. This phenomenon leads to increased power production, especially at high tip speed ratios. Similar trends were observed in high-fidelity CFD simulations [18, 19]. More recently, Senga et al. [20] used a lifting line free-vortex wake code to study the effect of tilt on VAWTs with different aspect ratios, while Kouaissah et al. [21] employed high-fidelity CFD to analyze a tilted H-shaped VAWT, elucidating the physics behind the increase in energy conversion. The majority of studies indicate that H-shaped VAWTs can achieve improved performance at a specific tilt angle, despite the complex aerodynamics inherent to this condition. To gain a comprehensive understanding of their energy-harvesting capabilities and accurately predict near-wake development, a high-resolution numerical scheme is needed. With high-fidelity we indicate a detailed modeling of the fully 3D wind rotor, making use of the URANS equations to model the aerodynamics, as proposed *e.g.* in [22]. RANS/URANS are still backbone of modern design, since their accuracy involves industrially acceptable CPU time at the expense of preliminary, ad-hoc, testing to assess the reliability of selected set-up. In this case, unsteady blade-resolved CFD simulations can serve as a good predictive tool, providing a detailed representation of complex flow fields. Hybrid RANS/LES will see future growing, already underway, for example to deal with flow features within the far wake.

As presented in the open literature, significant advantages are highlighted regarding the tilted condition, but further efforts are required to enhance to fill the gap with other technical solutions and foster the attractiveness of the VAWTs in offshore. This includes a thorough evaluation of potential optimized designs that can operate effectively under these conditions. This work aims to further advance in this direction by presenting a high-fidelity study on a newly optimized model called **HV3**, developed based on prior optimization research [23]. Some advantages identified in this previous optimization study led to the development of the case study, detailed in the following section. Design and operating rotor parameters directly determine the flow extraction capability and wake recovery. In the current investigation, the torque profile and power coefficient, at different spanwise position, are used to discuss the performance level. Viscous losses and vortical structures evolution are examined in detail and related to the near wake shape and its development. The relevant parameters such as the effective incoming flow, the swept area, local suction effects are evaluated to characterize the optimized HV3 machine. The overall local and global performance is also discussed for a large scale model under imposed tilt angle. The study is threefold relevant as: i) it quantifies the wind turbine performance with tight connection to the design, ii) it shows the potential harvesting capability at high Reynolds regime, iii) it gives indications of the wake establishment to be considered in a possible farm installation.

2 Case of Study

In order to facilitate a rapid understanding of the case of the study, it is essential to define the three H-shaped VAWT models that were presented and analyzed in the preceding work [23], reported in left-hand side of Figure 1.

H: is a standard H-shaped VAWT with a 20° tilt angle, which is an optimal angle value obtained in [21]). Analyzing this configuration served as a reference for the subsequent solutions.

HV1: is a modified design of the reference case by introducing a 20° coning angle in the upper part of the turbine to counteract the tilt angle, making the blade able to operate almost upright despite the overall tilt. The goal was to preserve the advantages of the lower section (harvesting energy both in upwind and downwind, as observed in [21]) while reducing the negative effects of tilt on the upper part, especially in the upwind region where torque is highest.

HV2: offered a compromise between H and HV1 solutions. The coning angle is increased by 10 degrees both in the upper and lower portions of the machine. The angle was introduced in the lower part to evaluate its impact in this portion, which

encounters undisturbed air both in upwind and downwind regions.

Building on the findings [23] and integrating the advantages of both HV1 and HV2, a new model, called **HV3**, has been developed and studied in this work. HV1 showed greater potential for energy capture in the upper region, thanks to its higher coning angle and increased swept area. In contrast, HV2 demonstrated performance improvements and a larger swept area in the lower portion, which is attributed to its coning angle there. As a result, **HV3** incorporates a 20° coning angle in the upper section and a 10° coning angle in the lower section, see Figure 1.
All models (H, HV1, HV2, and HV3) share identical geometric parameters, with variations occurring only in their coning angles, as shown in Figure 1. Each model features a NACA0021 airfoil profile and has a solidity value of 0.3. All models feature one holding strut due to a reduced aspect ratio which equals 1.2. The main geometric and operational characteristics are outlined in Table 1.

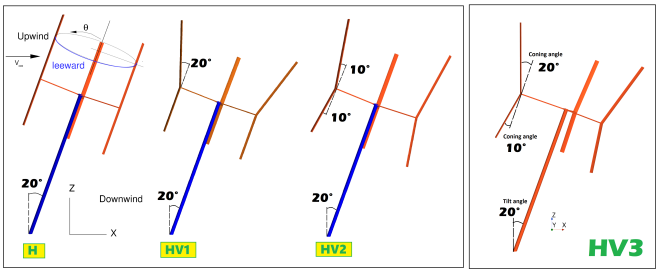

Figure 1: Previous analyzed wind turbine models [23], and the new HV3 model

The swept area for the HV3 model is determined using the same equation applied to the HV2 model, as detailed in [23]. Following a comparative analysis with the previous models, to evaluate the impact of the Reynolds number on the HV3 model and assess its performance at the utility-scale, three different scales were investigated: the so called **small** model (0.5-1kW power target, dimensions reported in 1), the **medium** one (the small model scaled by a factor of 20, power target of 500KW, Reynolds number around 3.5 Million), and finally the **large** one (scaled by a factor of 60, power target of 5MW, Reynolds number around 10 Million). The TSR condition has been selected in agreement to former studies. The rotating speed of revolution varied accordingly to compare different scalings of the rotor, at fixed free stream wind velocity.

3 Numerical methodology

High-fidelity simulations were performed on the three scales of the HV3 VAWT model, using the CFD solver STAR-CCM+. The flow model assumes the fluid behaves as an ideal, incompressible gas with constant thermophysical properties. To capture the fluid dynamics, the governing equations were discretized using Unsteady Reynolds-Averaged Navier-Stokes (URANS) modeling with second-order accurate schemes, supplemented by wall-resolved turbulence models. The $k-\omega$

	Small	Medium	Large
Lower blade part [m]	1.01	20.2	60.6
Upper blade part [m]	1.41	28.2	84.6
Rotor Radius at Strut [m]	1.01	20.2	60.6
Chord [m]	0.101	2.02	6.06
Rotation speed [rpm]	300	15	5
Wind speed [m/s]	9	9	9
Reynolds Number	180 K	3.5M	10M
TSR	3.54	3.54	3.54
Rated Power [kW]	0.5	$5{\cdot}10^2$	$5{\cdot}10^3$

Table 1: The main geometrical and operational parameters

SST turbulence model, developed by Menter [24] was selected (low-Re version for the small scale and high-Re for medium and large scales), given its proven capability to accurately predict complex vortical structures, as demonstrated in prior studies, including those by the authors [21, 25–28]. Choosing an appropriate time step is crucial for VAWT simulation accuracy. The turbine revolutions were divided into 720 intervals, a decision aligned with recommendations from other studies such as [26, 29]. At each time step, the system of governing equations was solved using an algebraic multigrid solver until the system reached an accuracy threshold of 10^{-5}. The simulations were performed on the high-performance computing cluster provided by the Norwegian Research Infrastructure Services (Sigma2). Each case required approximately two weeks hours of computational time relying upon 64 processors.

Simulations for the three scales continued until a periodic solution was achieved, typically around the 20th turbine revolution. To ensure time periodicity, the mean torque at the shaft was recorded and averaged over one revolution. The last five mean values were monitored closely, ensuring the relative error remained below 2%. Well-suited domain boundaries are essential to avoid artificial blockage effects and minimize computational costs, as suggested in [26]. Following this study's guidelines, the 3D domain was defined with an inlet boundary placed 4.5 diameters upstream of the shaft, an outlet at 3 diameters downstream, and lateral boundaries located 3 diameters away from the shaft. Vertically, the domain extended one turbine height above and below the turbine. Even though, the domain extents may appear to be small, they have been proven suited to deal with the blockage effects of the rotor in a former work of the authors. This issue is relevant to get a satisfactory approximation of the flow field, and prevent possible, undesired, numerical oscillations and not satisfactory performance predictions. Through proper sensitivity procedure led on a similar model (in terms of overall aerodynamic behavior and blockage effects), it was shown that the selected domain can provide a good description of the local and global flow performance parameters, see also [25] for details on the agreements of numerics against measurements.

Regarding the boundary conditions, a fixed freestream velocity with a turbulence intensity of 1% and a turbulent viscosity ratio of 1 was applied at the inlet surface, matching the wind tunnel experimental data used to validate the H-type model. Static pressure was prescribed at the lateral, down-

stream, and top boundaries, while a no-slip condition was imposed on solid (rotating) surfaces and the ground. For the sake of description of local flow behavior, the investigation of the model was carried out by considering spanwise slices defined along the blades, as illustrated in the right-hand side of Figure 2: 10 in the lower section and 14 in the upper section. This segmentation facilitates a detailed local evaluation of the rotor performance.

The computational grid has been defined following well established guidelines already assessed in terms of mesh coarseness ans quality. The sensitivity not reported here for the sake of brevity, has been carried out to obtain the minimum required elements number (approx 20 millions elements). The clustering of elements near solid wall is performed to fulfill the $y^+ \approx 1$ imposed by the selected turbulence model. A rotating region is defined through offset of the rotor geometry and coupled with stator, fixed region through sliding interface selection. The mesh is defined through polyhedral shaped elements, useful to reduce the overall computational cost, while preserving the discretization accuracy. Scaling up of the discrete domain followed the same guidelines and constraints.

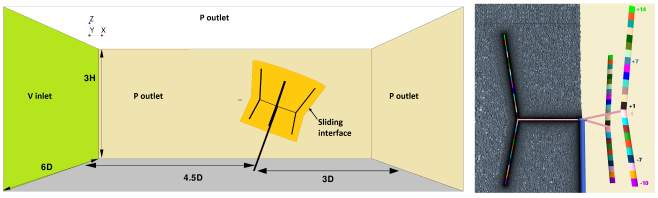

Figure 2: Domain, boundary conditions, mesh and blade slices numeration

The validation of the computational set-up presented in this section has been carried out on a similar wind rotor and reported in [30]. The relative per cent error on the C_P value computed near peak power condition, with operating parameters corresponding to those of the small model HV3, amounts to nearly 14% against measurements, with an uncertainties level of experiments of $\pm 7\%$. The local flow velocity field computed at near wake position were found in very good agreement with measurements, both in terms of shape and width, and blockage level.

4 HV3 Optimized model: Performance prediction

This section presents the performance of the new HV3 model in comparison to the results obtained for previous models. Table 2 summarizes the findings, including the overall power coefficient (C_P), the swept area for each model, and the relative increase compared to the baseline H model. The introduction of the coning angle leads to an enhancement in the power coefficient of nearly ten percent for HV3, in agreement with results already presented in [23], complemented by a significant increase in the swept area. The final expected performance enhancement for the novel HV3 model can be appreciated in the final power output, reaching an increase of 35%. We notice that the performance enhancement of the designed HV3 model can be related both to the blade coning angle and to the enlarged swept area. The two issues have a role, the former affects most directly the aerodynamics and thus the power coefficient variation. Instead the latter results into a major impact on overall viscous losses and power harvesting. At first glance, the HV2 and HV3 models share the same aerodynamic efficiency, with the latter taking advantage of larger active area. To obtain more detailed indications on the performance of HV3 against HV2 model, the local parameters of influence need to be considered separately. In fact, even though they highlight the same C_P value, different effective incoming velocity of the rotor upper part need to be considered, along with the increased available swept area. Therefore, deeper understanding of local flow features is needed. First, the power coefficient is considered in view of the torque profile as reported by Figure 3; the top part illustrates the local power coefficient for the small scale's HV1, HV2, and HV3 models. The computation of this parameter has been conducted using the local reference data pertaining to each spanwise slice. Due to geometric similarity, the local performance of HV3 shows good agreement with HV2 in the lower section (slices -10 to -1) and aligns well with the upper section of HV1. This indicates that HV3 effectively captures the performance characteristics of both HV2 and HV1 across different regions of the turbine, as intended by the combination of both designs. The same trends is shared by all the models in the region in between slice -1 and slice +1, where the viscous losses of the connecting strut determine expected performance hole. This C_P reduction stems from slices ± 2 owing to the actual inclined position of the wind turbine models.

Table 2: Power coefficient, swept area and gathered power, small-scale.

Rotor	C_P	$C_P(\%)$	A_{sw}	$A_{sw}(\%)$	P [W]	Δ(P)%
H	0.232	-	5.59	-	540	-
HV1	0.246	+6	6.73	+20	693	+28
HV2	0.257	+11	6.61	+18	711	+32
HV3	**0.255**	**+10**	**6.98**	**+25**	**729**	**+35**

The observed trend in local C_P is inherently linked to the similarity in the moment coefficient along the span. The middle Figure 3 shows the slice at -5, representative of the lower section of the turbine, where a notable similarity between HV2 and HV3 is evident. In this machine portion, C_M is produced both in the upwind and downwind zones due to the undisturbed flow conditions. In contrast, the slice at +13 Figure 3(bottom) pertains to the upper section, where HV3 is equivalent to HV1. The difference observed in the maximum values of C_M-5 and C_M+13 in the upwind region (around 90 degrees) is related to the fact that the machine portion at position +13 operates in a nearly vertical orientation in this area, whereas the slice at -5 operates with an oblique angle, which combines the turbine tilt angle and the coning angle.

VAWT behaviour must be evaluated also in terms of near wake development and evolution; Figure 4 displays the non-dimensional streamwise velocity at two selected $X/D = const$

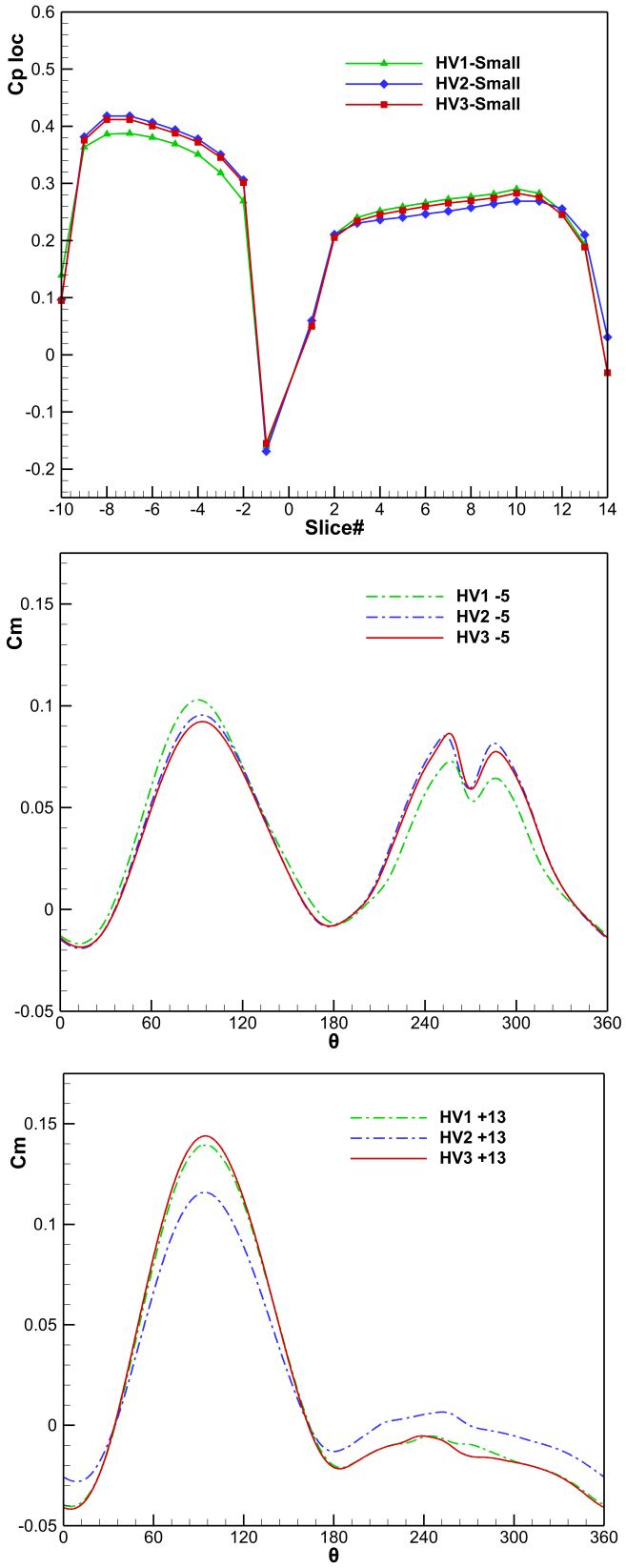

Figure 3: Small models: local C_p (top), C_M at slices -5 & +13 (middle/bottom).

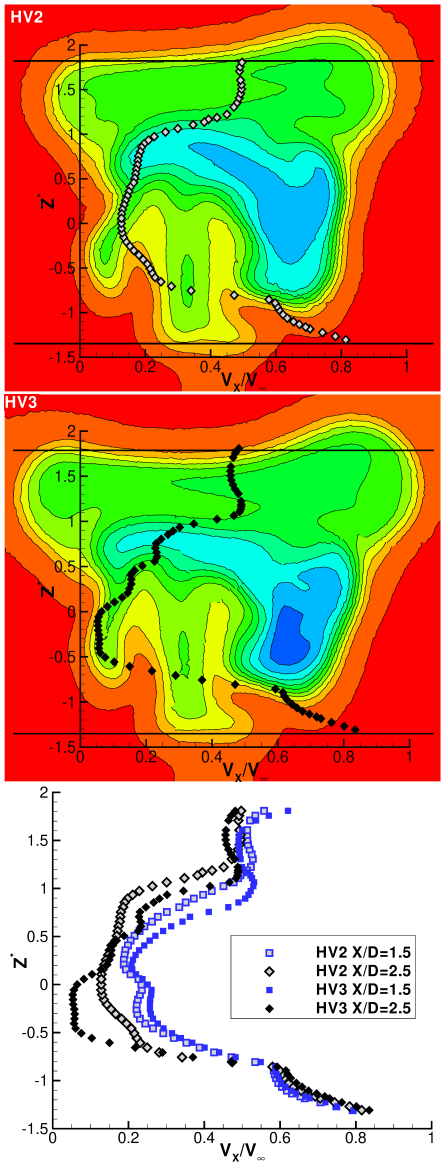

Figure 4: Near wake streamwise velocity: HV2/HV3 at $X/D = 2.5$ (top/mid), minimum velocity defect at $X/D = 1.5, 2.5$ (bottom)

planes, selected in the near wake region. Even though the local and global C_P of HV2 and HV3 closely resemble one another, different wake establishment takes place. The velocity maps are reported along with the tracking of minimum velocity value as a function of the spanwise position. Different wake morphology appears: i) the HV3 model stems into narrower wake, though deeper than the HV2 one, ii) moving downstream the lower part of HV3 results into a slower evolution trend (see Figure 4 right).

5 HV3: Utility-scale evaluation

This section contains a comparative analysis of the HV1, HV2, and HV3 models at the large scale, followed by an examination of the HV3 model across the three previously defined scales: small, medium, and large. Table 3 summarizes the overall efficiency, swept area, and the final enhanced harvested power by comparing the three large models. In addition, the left side of Figure 5 compares the local C_P of the large models, confirming the similarity of HV3 to the HV2 and HV1 models in the lower and upper portions, respectively. Overall, the results align with and support previous findings and discussions conducted on small scales. However, the 33% increase in the final power of the large HV3 model compared to a standard H-shaped tilted solution represents an encouraging achievement to eventually reduce the LCOE, especially considering that the dimensions remain unchanged, except for the coning angle.

Table 3: Power coefficient, swept area and gathered power, large-scale.

Rotor	C_P	$C_P(\%)$	A_{sw} m^2 x10^3	$A_{sw}(\%)$	P [MW]	Δ(P)%
H	0.33	-	20.6	-	2.88	-
HV1	0.34	+3	24.2	+20	3.60	+25
HV2	0.36	+10	23.8	+18	3.75	+30
HV3	**0.35**	**+9**	**25.5**	**+24**	**3.83**	**+33**

Understanding how the performance varies with the machine scale is a key objective of this study. The performance metrics for both small and large scales have been outlined in Tables 2 and 3, respectively. For the medium model, the achieved power coefficient is **0.31**, with a swept area of **2792** m^2 and a final power output of approximately **350 kW**. The bottom side Figure 5 compares instead the local power coefficients across the three selected scales. Notice that the reduction of viscous effects is more pronounced in the lower portion of the machine and near the holding strut position. In these regions, the blades engage with undisturbed air in both the upwind and downwind regions and this fact results into a more effective incoming velocity. This behavior is linked to the combined effect of the coning angle and imposed tilt position that determines higher approaching velocity, and thus a reduced influence of viscous losses. This outcome suggests the potential of large scale VAWTs under proper design, scale and operating conditions.

In contrast, the blades in the upper section interact with undisturbed air only in the upwind area, while the downwind blade encounters wake effects, limiting the reduction of viscous effects with an increase in scale. These observations are more appreciable when analyzing the trend of the moment coefficient for slices -7 and +5, which are representative of the two sections of the turbine, as illustrated in Figure 6. However, the comparison of the local power coefficient reported on the bottom-located Figure 5 indicates that the viscous losses associated with the struts are most effectively reduced by increasing the scale, see the value of the Cp at the slice-1 which includes the strut itself. The near-wake establishment closely

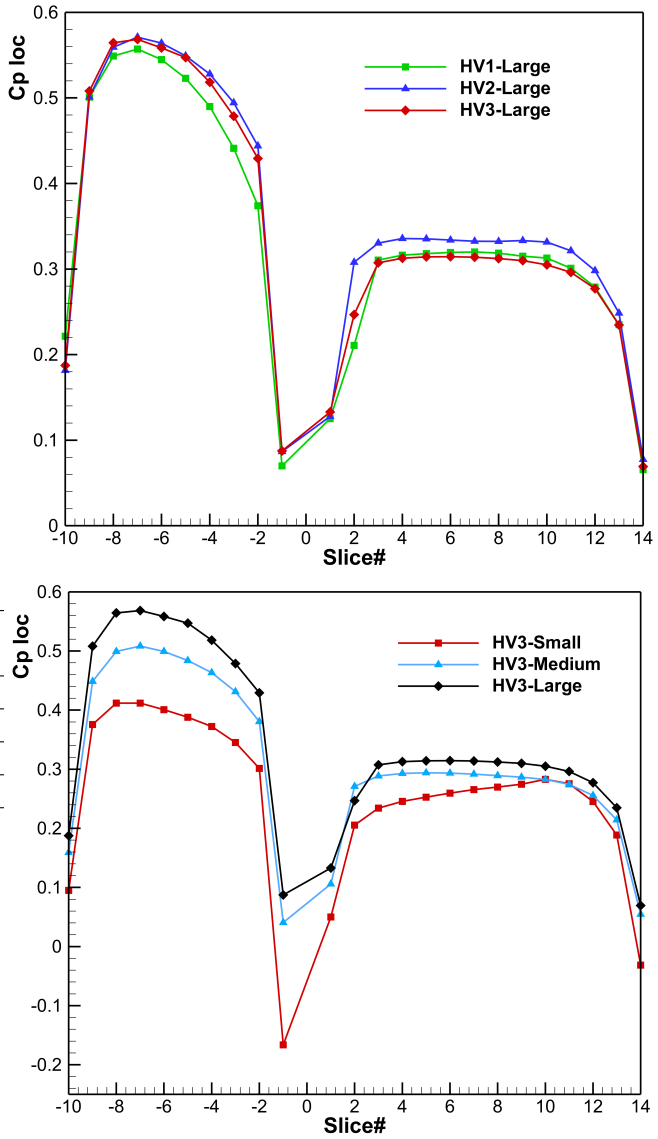

Figure 5: Local C_p: Comparison of large models (top), HV3 at the three scales (bottom)

depends on the selected design. The width and depth of the wake, behind the rotors, in the lower and upper parts of the HV3 machine can be compared to previous H1 and H2 designs. The average contours of the streamwise velocity computed for the three models are displayed in Figure 7 at a cross-section placed at $X/D = 2.5$. The wake downstream of the

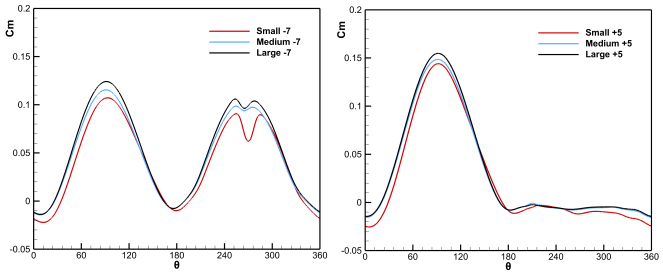

Figure 6: **HV3**: Cm-7 and Cm+5 (left and right) for the three scales

wind turbine is shaped by both its design and operating conditions, expanding and evolving as the flow progresses.

In our case, the wake predicted by the HV3 model, as expected by design, combines characteristics from both the HV2 and HV1 models. In the lower region, HV3 closely mirrors HV2, indicating similar flow dynamics and energy capture potential. Meanwhile, in the upper region, HV3 more closely resembles HV1, suggesting that the flow behavior and wake development in that area align with HV1 characteristics. The spanwise evolution of the wake is shown in Figure 8.

At the strut section, $Z^* = 0$ relevant asymmetric distribution of the velocity defect can be observed. Instead, near the blade tip position $Z^* = 1$ the wake reverted back to a nearly symmetric condition. These outcomes indicate that the leeward side experiences a faster re-energized wake compared to the windward side. Upward vertical movements are therefore suggested in this region. The velocity profiles of the large-scale rotor closely match those of the small model.

6 Conclusions

This study has numerically investigated the aerodynamic performance and energy-harvesting potential of the newly developed HV3 VAWT, designed to operate under tilted conditions. The HV3 model incorporates elements from previous HV1 and HV2 designs, combining features such as modified stacking lines and an optimized coning angle to maximize energy conversion. The goal was to leverage the advantages of undisturbed airflow in the lower section while minimizing the effects of blade inclination in the upper section during the upwind phase. Another objective of the work was the study of potential capability of VAWTs at large scale applications. Numerical predictions have been presented relying upon three-dimensional computations performed with well-resolved CFD unsteady numerical set-up.

Key findings obtained on the investigated HV3 model include the following topics:

- The HV3 rotor exhibits a combination of advantages seen in both HV1 and HV2 models, resulting in a well-balanced design that offers up to a 35% increase in power generation over standard H-type turbines. These improvements are evident both in small and large-scale applications.

- The reduction of viscous effects (high Reynolds number) is remarkable in the zone where the turbine's blade encounters undisturbed air and at the strut region.

- Analogous to HV1 and HV2, the case study of HV3 demonstrates an enhanced vertical air motion, which could contribute to improved wake recovery, particularly

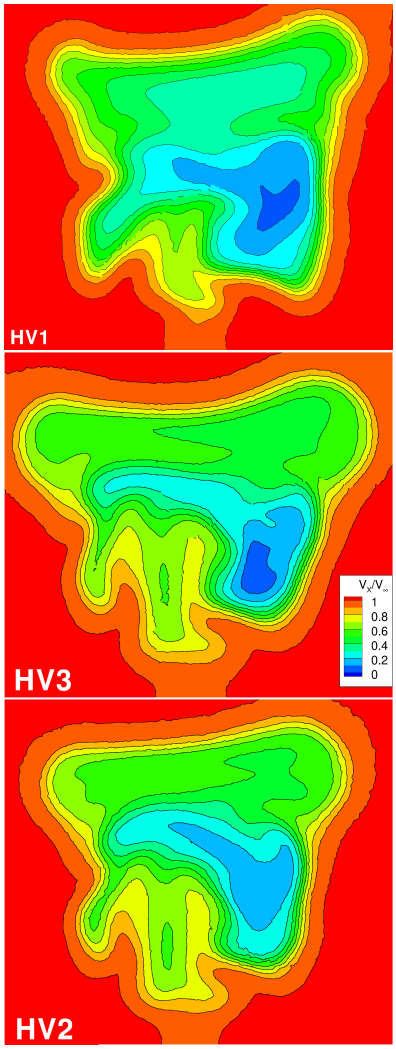

Figure 7: Small-scale models: near wake velocity defect V_x/V_{inf} at $X/D_{eq} = 2.5$ section. HV1 (top), HV3 (middle) and HV2 (bottom)

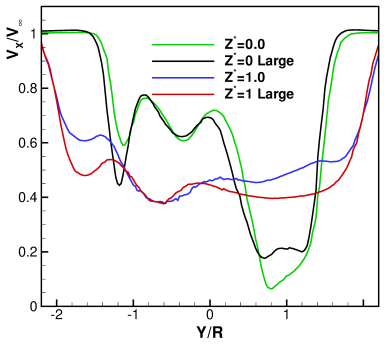

Figure 8: Near wake profiles over $X/D = 2.5$ section, at two different span positions, for the small and large HV3 models

in the lower region of the turbine.

These observations could be further extended by means of an additional design study involving more key parameters complementing the blade definition. Given the complex and unsteady nature of the flow around the HV3 turbine, further multidisciplinary research is recommended to refine and strengthen the design. Further future investigation aim at fully exploiting the potential for sustainable energy generation needs to consider the rotors coupling and interaction.

Nomenclature

a	axial induction factor
C_l, C_d	sectional lift and drag coefficients
C_P	power coefficient
p	static pressure
T	thrust
w	relative velocity
Z	blade count

Greek symbols

α	angle of attack
λ	tip speed ratio
ρ	fluid density
σ	solidity
Ω	rotor angular velocity

Subscripts

h	hub

Superscripts

$\widehat{\ }$	dimensionless quantity

Acronyms

CFD	computational fluid dynamics
FSP	front stagnation point

References

[1] *Global Offshore Wind Report.* https://wfo-global.org/wp-content/uploads/2024/04/WFO-Report-2024Q1.pdf. Accessed: September 2024.

[2] A. Ghigo, E. Faraggiana, G. Giorgi, G. Mattiazzo, and G. Bracco. "Floating Vertical Axis Wind Turbines for offshore applications among potentialities and challenges: A review". In: *Renewable and Sustainable Energy Reviews* 193 (2024).

[3] *GWEC report.* https://gwec.net/report-outlines-enormous-potential-for-floating-offshore-wind-in-energy-transition/. Accessed: September 2024.

[4] M. Islam, S. Mekhilef, and R. Saidur. "Progress and recent trends of wind energy technology". In: *Renewable and Sustainable Energy Reviews* 21 (2013), pp. 456–468. ISSN: 1364-0321. DOI: https://doi.org/10.1016/j.rser.2013.01.007.

[5] W. Tjiu, T. Marnoto, S. Mat, M. H. Ruslan, and K. Sopian. "Darrieus vertical axis wind turbine for power generation I: Assessment of Darrieus VAWT configurations". In: *Renewable Energy* 75 (2015), pp. 50–67.

[6] J. O. Dabiri. "Potential order-of-magnitude enhancement of wind farm power density via counter-rotating vertical-axis wind turbine arrays". In: *Journal Renewable and Sustainable Energy* 3.043104 (Sept. 2011).

[7] F. Ottermo and H. Bernhoff. "An upper size of vertical axis wind turbines". In: *Wind Energy* 17 (2014), pp. 1623–1629.

[8] B. Hand and A. Cashman. "A review on the historical development of the lift-type vertical axis wind turbine: From onshore to offshore floating application". In: *Sustainable Energy Technologies and Assessments* 38 (2020), pp. 1–11.

[9] W. Tjiu, T. Marnoto, S. Mat, M. H. Ruslan, and K. Sopian. "Darrieus vertical axis wind turbine for power generation II: Challenges in HAWT and the opportunity of multi-megawatt Darrieus VAWT development". In: *Renewable Energy* 75 (2015), pp. 560–571. ISSN: 0960-1481. DOI: https://doi.org/10.1016/j.renene.2014.10.039.

[10] B. Hand and A. Cashman. "Conceptual design of a large-scale floating offshore vertical axis wind turbine". In: *Energy Procedia* 142 (2017). Proceedings of the 9th International Conference on Applied Energy, pp. 83–88. ISSN: 1876-6102. DOI: https://doi.org/10.1016/j.egypro.2017.12.014.

[11] W. Xu, G. Li, and Y. Li. "Feasibility analysis of aerodynamic characteristics for vertical-axis turbines in offshore: A comprehensive analysis on scale and design of wind system". In: *Ocean Engineering* 285 (2023), p. 115406. ISSN: 0029-8018. DOI: https://doi.org/10.1016/j.oceaneng.2023.115406.

[12] S. Mertens, G. van Kiuk, and G. van Bussel. "Performance of an H-Darrieus in the skewed flow on a roof". In: *ASME Journal of Solar Energy Engineering* 125 (Sept. 2003), pp. 433–440.

[13] C. J. S. Ferreira, G. J. W. Van Bussel, and G. A. M. Van Kuik. "Wind tunnel hotwire measurements, flow visualization and thrust measurement of a VAWT in skew". In: *Journal of Solar Energy Engineering, Transactions of the ASME* 128.4 (2006), pp. 487–497.

[14] C. Simao Ferreira, K. Dixon, C. Hofemann, G. van Kuik, and G. van Bussel. "VAWT in skew: Stereo-PIV and vortex modeling". In: *47th AIAA aerospace sciences meeting including the new horizons forum and aerospace exposition*. 2009, p. 1219.

[15] L. Battisti, E. Benini, A. Brighenti, S. Dell'Anna, M. R. Castelli, V. Dossena, G. Persico, U. Paulsen, and T. Pedersen. "Wind Tunnel Testing of the DeepWind Demonstrator in Design and Tilted Operating Conditions". In: *Energy* 111 (2016), pp. 484–497.

[16] K. Wang, M. O. L. Hansen, and T. Moan. "Model improvements for evaluating the effect of tower tilting on the aerodynamics of a vertical axis wind turbine". In: *Wind Energy* 18.1 (2015), pp. 91–110.

[17] F. Scheurich and R. Brown. "Vertical-axis wind turbines in oblique flow: sensitivity to rotor geometry". In: *EWEA Annual event (formerly known as EWEC)* (2011).

[18] A. Orlandi, M. Collu, S. Zanforlin, and A. Shires. "3D URANS analysis of a vertical axis wind turbine in skewed flows". In: *Journal of Wind Engineering and Industrial Aerodynamics* 147 (2015), pp. 77–84.

[19] A. M. Chowdhury, H. Akimoto, and Y. Hara. "Comparative CFD analysis of Vertical Axis Wind Turbine in upright and tilted configuration". In: *Renewable Energy* 85 (2016), pp. 327–337.

[20] H. Senga, H. Umemoto, and H. Akimoto. "Verification of Tilt Effect on the Performance and Wake of a Vertical Axis Wind Turbine by Lifting Line Theory Simulation". In: *Energies* 15 (2022).

[21] O. Kouaissah, N. Franchina, and G. Persico. "A computational study on the performance and wake development of a H-Shaped VAWT rotor". In: *Renewable Energy* Accepted (2024), pp. -.

[22] M. H. A. Madsen, F. Zahle, N. N. Sørensen, and J. R. R. A. Martins. "Multipoint high-fidelity CFD-based aerodynamic shape optimization of a 10 MW wind turbine". In: *Wind Energy Science* 4.2 (2019), pp. 163–192. DOI: 10.5194/wes-4-163-2019.

[23] O. Kouaissah, N. Franchina, and G. Persico. "A Computational Fluid Dynamics Study on the Performance of Modified H-Shaped VAWTs for Tilted Operation Condition". In: *Journal of Engineering for Gas Turbines and Power* 147 (2024), p. 051017.

[24] F. R. Menter. "Two-equation eddy-viscosity turbulence models for engineering applications". In: *AIAA Journal* 32.8 (1994), pp. 1598–1605.

[25] N. Franchina, O. Kouaissah, G. Persico, and M. Savini. "Three-dimensional CFD simulation and experimental assessment of the performance of a H-shaped vertical axis wind turbine at design and off-design conditions". In: *Int. J. Turbomach. Propuls. Power* 4(3),30 (2019). DOI: https://doi.org/10.3390/ijtpp4030030.

[26] N. Franchina, G. Persico, and M. Savini. "2D-3D Computations of a Vertical Axis Wind Turbine Flow Field: Modeling Issues and Physical Interpretations". In: *Renewable Energy* 136 (2019), pp. 1170–1189.

[27] O. Kouaissah, N. Franchina, and G. Persico. "3D CFD study of a DeepWind demonstrator at design, off-design and tilted operating conditions". In: *Energy* 291 (2024), p. 130313. ISSN: 0360-5442. DOI: https://doi.org/10.1016/j.energy.2024.130313.

[28] N. Franchina, O. Kouaissah, G. Persico, and M. Savini. "Three-dimensional modeling and investigation of the flow around a troposkein vertical axis wind turbine at different operating conditions". In: *Renewable Energy* 199 (2022), pp. 368–381.

[29] F. Balduzzi, A. Bianchini, G. Ferrara, and L. Ferrari. "Dimensionless numbers for the assessment of mesh and timestep requirements in CFD simulations of Darrieus wind turbines". In: *Energy* 97 (2016), pp. 246–261.

[30] N. Franchina, G. Persico, and M. Savini. "Three-dimensional unsteady aerodynamics of a H-shaped vertical axis wind turbine over the full operating range". In: *Journal of Wind Engineering & Industrial Aerodynamics* 206 (2020).